Inverse-Leidenfrost phenomenon on nanofiber mats on hot surfaces

Christina M. Weickgenannt,[1,2] Yiyun Zhang,[3] Suman Sinha-Ray,[3] Ilia V. Roisman,[1,2] Tatiana Gambaryan-Roisman,[2,4] Cameron Tropea,[1,2,*] and Alexander L. Yarin[2,3,†]

[1]*Institute of Fluid Mechanics and Aerodynamics, Technische Universität Darmstadt, D-64287 Darmstadt, Germany*

[2]*Center of Smart Interfaces, Technische Universität Darmstadt, D-64287 Darmstadt, Germany*

[3]*Department of Mechanical and Industrial Engineering, University of Illinois at Chicago, M/C 251, Chicago, Illinois 60607-7022, U.S.A.*

[4]*Institute of Technical Thermodynamics, Technische Universität Darmstadt, D-64287 Darmstadt, Germany*

(Received 14 April 2011; published 13 September 2011)

The Leidenfrost effect is a technically and industrially important phenomenon that severely restricts heat removal from high-heat-flux surfaces. A simple remedy to the Leidenfrost effect is provided by polymer nanofiber mats created and deposited by electrospinning on stainless steel surfaces. The influence of nanofiber mats on hydrodynamics and cooling efficiency of single drop impact onto hot surfaces has been investigated experimentally. The evolution of the drops has been recorded by a high-speed complimentary metal-oxide semiconductor camera, whereas the cooling temperature was measured by a thermocouple. A remarkable phenomenon was discovered: a mat of polymer nanofibers electrospun onto a heater surface can completely suppress the Leidenfrost effect, thereby increasing the rate of heat removal from the surface to the liquid drops significantly. The "inverse-Leidenfrost" effect is described qualitatively and quantitatively, providing clear physical reasons for the observed behavior.

DOI: 10.1103/PhysRevE.84.036310 PACS number(s): 47.55.dr, 44.35.+c, 47.56.+r

I. INTRODUCTION

The Leidenfost effect, described in 1756, is familiar to anyone who once sprinkled drops of water on a very hot skillet or a pan [1,2]. At temperatures about 150°C, instead of an almost instantaneous flash evaporation, the Leidenfrost effect surprisingly allows water droplets to survive for several minutes and skid and roll over the hot pan surface. Due to the initial intense evaporation at the bottom of the drop in contact with the hot skillet, a vapor layer between the drop and the hot surface is generated with a pressure sufficient to levitate the drop (Fig. 1).

The Leidenfrost effect is not only a classical demonstration of kitchen physics but also a technically and industrially important phenomenon that severely restricts heat removal from high-heat-flux surfaces, since thermal conductivity through the vapor layer is negligibly small compared to the latent heat of water that might be exploited otherwise to remove heat. The behavior of individual cold droplets impinging onto hot surfaces determines directly the efficiency of spray cooling systems, which are presently one of the most effective methods for cooling of high heat flux surfaces. Spray cooling is a valuable alternative in extreme cases for microelectronics, optoelectronics, or radiological devices, for example, for cooling in unmanned aerial vehicles (UAVs) [3,4]. The tremendous cooling potential of this technology is associated with liquid evaporation at the hot surface. Its efficiency is strongly affected by the hydrodynamics and heat transfer associated with drop impact onto hot surfaces.

While the basic hydrodynamics of drop impact in the isothermal case is mainly understood [5], the accurate description of drop impact onto hot surfaces remains a challenging problem. Various aspects of this phenomenon have been investigated experimentally, namely heat transfer associated with drop impact [6], breakup probability [7], and the limiting temperature resulting in a drop rebound [8]. The phenomena of drop impact onto hot surfaces are influenced significantly by the contact temperature [9], which is a function of the initial temperatures of the wall, and drop, their thermal diffusivities, the wall thickness, and the Prandtl number of the liquid. In Ref. [10] an expression for the contact temperature has been obtained from the analytic solution of the full Navier-Stokes equations combined with the thermal balance equation for fast spreading drops. If the wall temperature is high enough, the contact temperature exceeds the liquid saturation temperature. In this case the drop spreading is followed by intensive evaporation and boiling. In such regimes the heat transfer between the wall and drop is very high. On the other hand, if the contact temperature is significantly higher than the liquid saturation temperature, the Leidenfrost effect sets in [1,11] (cf. Fig. 1), droplets levitate, and heat transfer from the wall is significantly hindered by the intermediate vapor layer. Moreover, the high pressure in the vapor layer leads to the instability of spreading liquid drops accompanied by their shattering and the formation of a cloud of small secondary droplets. A recent comprehensive review [12] shows that the dynamic Leidenfrost temperature, corresponding to the transition to the Leidenfrost regime, is a function of drop impact parameters. Abundant literature devoted to the Leidenfrost effect continues to expand at a steady pace [13,14] even though today a comprehensive theory (for example, a reliable prediction of the skittering speed) is still absent. However, the driving mechanism of the Leidenfrost effect depicted in Fig. 1 is already well understood.

The dramatic reduction of heat removal rate in the film boiling regime (above the Leidenfrost temperature) is one of the main challenges of spray cooling of high-temperature surfaces. One attractive way to enhance heat removal rate

*ctropea@sla.tu-darmstadt.de
†ayarin@uic.edu

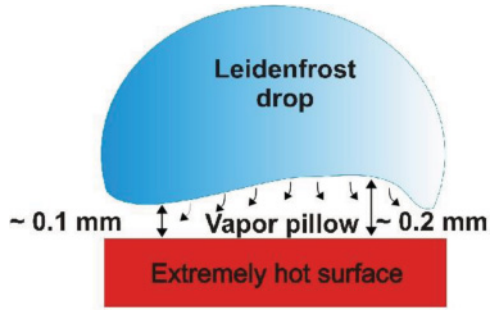

FIG. 1. (Color online) Leidenfrost effect: water droplet levitating on a vapor pillow above a very hot surface.

is associated with textured substrates, in particular, different types of rough, structured, or coated surfaces, which affect the outcome of a drop impact onto cold and hot surfaces [15–17].

One of the recently discovered and very promising methods for controlling hydrodynamics of drop impact and enhancing heat removal from a hot wall to a cold drop is associated with electrospun polymer nanofiber mats. Such mats consist of individual polymer or metal-plated fibers of submicron diameters, which are randomly orientated in the mat plane and consist of multiple nanofiber layers [18,19]. They can be produced on any conductive surface and have a strong adhesion to the hot surfaces even at temperatures as high as 300°C. It has been recently shown that such nano-textured surfaces significantly modify the outcomes of drop impact and dramatically enhance the heat removal rate [20–23]. They practically eliminate the receding motion of the contact line and bouncing on cold and hot surfaces. Furthermore, liquid coolants penetrate into nanofiber mats and spread inside them over a very large area, which remains wetted during a period of about 0.1–1 s. As a result, nano-textured surfaces covered with nanofiber mats dramatically increase cooling efficiency of individual drop impacts compared to that of drop impacts on bare metal surfaces for temperatures up to 172°C.

The aim of the present study is to investigate the influence of nanofiber coatings on drop impact onto very hot surfaces within the Leidenfrost regime. We study the effect of the nano-textured electrospun coatings on the hydrodynamics of drop impact and the corresponding cooling efficiency. The experimental method is described in Sec.II. The main results and discussion are presented in Sec. III, while Sec. IV is devoted to some additional phenomena observed in the experiments. Conclusions are drawn in Sec. V.

II. EXPERIMENTAL METHOD

Nanofiber mats used in the present experiments were produced by electrospinning [18,19,24]. The nanofiber mats were electrospun from PAN [poly(acrylonitrile)], a partially wettable polymer. In some cases nanofiber mats contained carbon black nanoparticles (CB) which enhances roughness of individual nanofibers. Square samples of nanofiber mats with a side length of about 4 cm, thickness of the order of several hundred micrometers and porosity of the order of 90–95% were produced. Nanofiber mats were electrospun on stainless

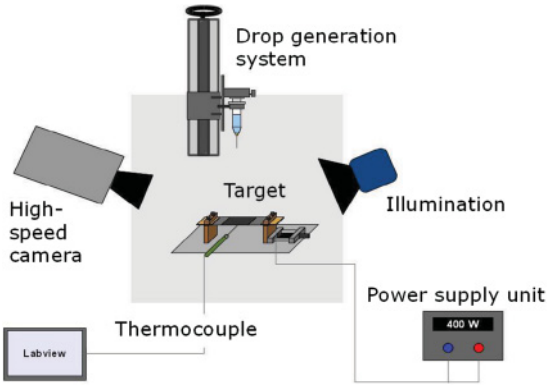

FIG. 2. (Color online) Experimental setup for drop impact onto nanofiber mats.

steel foils attached to a grounded electrode. The thickness of the foils was 50 μm.

A sketch of the experimental setup is shown in Fig. 2. The main components were a mounting device with an integrated foil heating system, a drop generation system, a high-speed complimentary metal-oxide semiconductor (CMOS) camera, and a temperature measurement system. The nano-textured foils were mounted in a device that drew them taught, counteracting the thermal expansion at high temperatures. The fastening clamps on the ends were also used for electrical heating of the foils. A medical syringe with a stainless steel needle was used for drop generation. The needle was flat tipped. The syringe was manually operated in a way where a drop could form at the needle tip, detach under its own weight, and be accelerated by gravity. The drop diameter was about $D_0 = 2$ mm $\pm$ 0.3 mm. This size typically corresponds to drops dripping from a needle due to gravity. A high-speed CMOS camera (Photron Fastcam 1024 PCI) was used to measure the initial drop diameter and impact velocity and observe the overall shapes of the spreading drops above the hot surface. The camera was aligned at an angle of 40° with respect to the horizontal. This experimental setup is similar to the one described in Ref. [23] which was used at foil temperatures up to 140°C [23], albeit the method of measuring the foil temperature differed in the present case. In particular, in Ref. [23] the temperature of the back side of the foil was measured by an infrared camera positioned underneath the foil. The experimental observations based on the comparison of the infrared and video images in Ref. [23] revealed the following two peculiarities of the process that allow simplification of the observation system. First, the wetted area inside the nanofiber mat had a circular shape with the center at the drop impact point and also exhibited a uniform temperature. The wetted area expanded after drop impact, reached its maximum and after that receded from the periphery to the center. In such a situation the evaporation time of a drop can be determined by measuring the foil temperature at the impact position alone. Second, the fact that the temperature field is approximately homogeneous over the entire wetted area both on bare steel foils, as well as on the foils coated with nanofiber mats allows the temperature measurement to be conducted at a single representative point. In particular, in the present experiments a single thermocouple of type K with a diameter of 0.5 mm

was pressed onto the back side of the foil under the drop impact point. A soldered connection of the thermocouple onto the foil was problematic because of the high temperature encountered. It is well known that such a method can lead to a systematic error up to 4°C, caused by the thermal resistance between the thermocouple joint and the foil surface. However, these measurements can be reliably used for determination of the cooling dynamics and for comparison between different cases. The data has been acquired and analyzed using the LABVIEW software. The following experimental procedure was followed. The heater was turned on at a fixed electric power, and the surface temperature was allowed to reach a steady state before a drop impacted from a height $H = 15$ cm above the target. From the previous experiments it is known that at this impact height the kinetic energy is high enough to ensure that the drop reaches the foil surface and low enough that no splash at the surface occurs. To measure the initial foil temperature, the thermocouple on the bottom side of the foil was used. In order to observe the details of drop impact during the initial drop deformation and spreading, the phenomenon has been captured by the high-speed CMOS camera with a frame rate of 30 kHz. To capture both drop spreading and evaporation processes, which take much longer, the lower frame rate of 125 Hz has been chosen.

The recording frequency of the thermocouple was 5 Hz. The camera and temperature measurement system were not synchronized in these experiments. The focus of the experiments was on the hydrodynamics of drop impact. The experiments were performed in the foil initial temperature range $60°C < T_{foil,init} < 300°C$ with an increment of 40°C and with nanofiber mat thicknesses in the range $0.15 \text{ mm} < h < 1.5 \text{ mm}$.

III. RESULTS AND DISCUSSION

A. Drop impact onto hot bare steel foils: The Leidenfrost effect

Typical drop impact outcomes on bare metal surfaces for different temperatures and experimental fluids were reported, for example, in Ref. [25]. It was shown that the onset conditions of nucleate boiling, transition boiling, and film boiling regimes are not exclusively controlled by the contact temperature but also by the properties of the heated surface, by the ambient pressure, and by the impact parameters. For different experimental setups and experimental conditions, different outcomes can be observed at the same temperature.

We begin reporting our results by examining drop impact onto bare steel foils under different experimental conditions, which will be used as a reference point in comparison with drop impacts onto nano-textured surfaces. Figure 3 illustrates the outcomes of water drop impacts at different initial foil temperatures. In each case the drop evolution after the impact is depicted at the same time instances after the first contact between the drop and the foil surface in order to demonstrate the influence of the foil temperature on hydrodynamics.

Figure 3(a) shows the impact of a water drop onto a bare steel foil at an initial foil temperature of 60°C. The drop impact is followed by spreading and receding of liquid over the surface. After the receding stage, which is driven by surface tension, the liquid drop reaches a quasi steady state. Subsequently, the drop height and contact angle gradually decrease because of the evaporative mass loss while the contact line remains completely pinned. Shortly before the end of the evaporation process the contact line de-pins, and the drop shows an additional appreciable shrinkage. In this case, as, in general, for temperatures below the boiling temperature of the liquid, the outcomes of drop impact are qualitatively

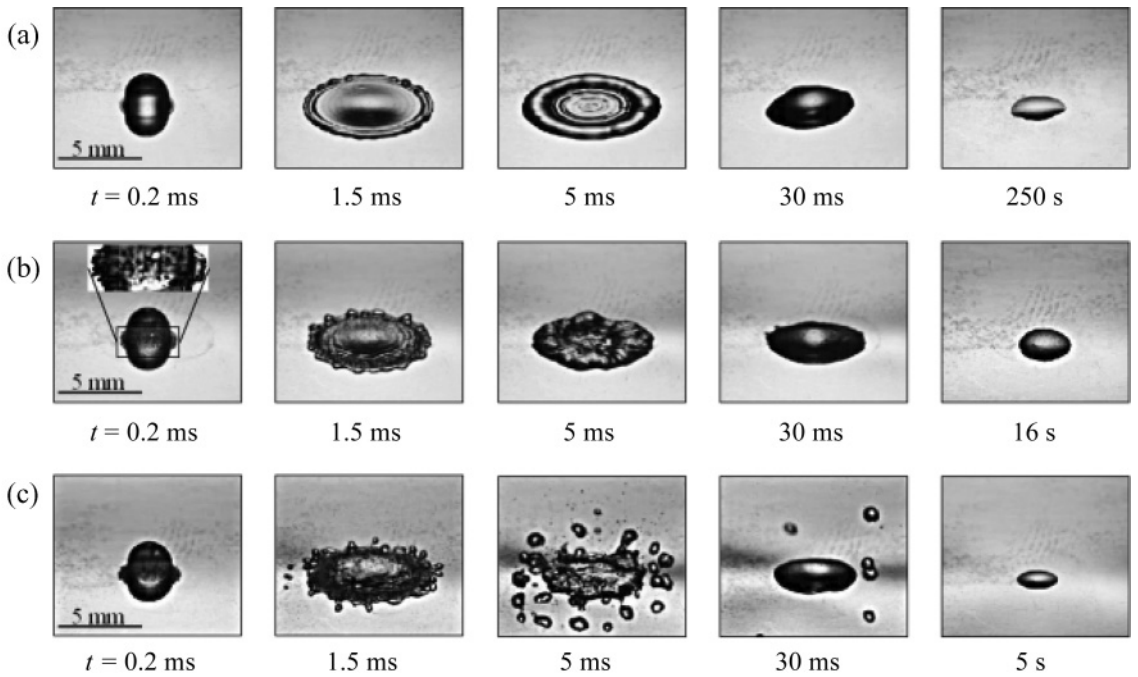

FIG. 3. Water drop impact on a bare steel foil at different initial foil temperatures. The initial foil temperature $T_{foil,init}$ is equal to (a) 60°C, (b) 220°C, and (c) 300°C.

comparable with the outcomes of drop impact onto unheated surfaces.

Significant differences in the outcomes of drop impacts onto hot bare steel foils in comparison to those for the drop impacts onto unheated bare foils were first observed in our experiments at an initial foil temperature of 220°C [see Fig. 3(b)]. In the first image of the sequence shown in Fig. 3(b), corresponding to the time instant $t = 0.2$ ms after drop impact, tiny bubbles at the interface between the drop and hot foil are visible (see enlarged section), which is typical for nucleate boiling. Then, in the spreading stage, the drop experiences perturbations due to capillary waves excited by boiling. Nevertheless, there is not yet drop fragmentation or levitation at this temperature; the drop stays intact and wets the foil. This is perhaps due to the fact that after drop impact the foil temperature decreases significantly below the temperature range corresponding to significant bubble nucleation.

For drop impact onto the bare stainless steel foil at an initial temperature of 300°C, the droplet shatters into secondary droplets and several tiny satellites [cf. Fig. 3(c)]. The atomization process is driven by a high pressure in the vapor below the drop at such high temperatures. Additionally, vapor recoil is probably a source of strong surface perturbations resulting in breakup into a multitude of tiny droplets. Those droplets are then accelerated away from the primary drop. The core of the primary drop during and after droplet shedding stays at the foil surface. It is emphasized that even though there is still some liquid left on the foil surface after the primary drop scattering, the cooling potential is reduced dramatically in this case. The contact area between the hot surface and the liquid is greatly reduced in comparison with the cases below the Leidenfrost point, the amount of liquid evaporating at the surface is reduced, and, as a result, the cooling is much less efficient.

Similar drop impact experiments with a bare heated steel foil have been performed with ethanol as a test liquid. Its saturation temperature, latent heat of evaporation and surface tension are lower than those of water, which leads to the intensification of the scattering effects at high temperature in comparison to those described before. In Fig. 4 the outcomes of ethanol drop impact at three initial foil temperatures are illustrated. It is seen that the spreading behavior of an ethanol drop on a stainless steel foil heated up to 60°C is qualitatively similar to that of a water drop [Fig. 3(a)]. The ethanol drop spreads, recedes, and stays in a stationary position until it fully evaporates. The most visible differences in comparison to a water drop impact at an initial foil temperature of 60°C is the reduction of the contact angle and an increase of the spreading velocity and the maximal spread-out contact diameter.

As a consequence of the lower saturation temperature (or higher volatility) and lower surface tension of ethanol in comparison to water, the onset of the nucleate boiling occurs already at an initial foil temperature of 140°C. By increasing the initial foil temperature up to 180°C, the Leidenfrost regime is nearly reached, as is depicted in Fig. 4(b). Surfaces at higher initial temperatures supported ethanol drops in the stable film boiling regime, in which the drops are levitated over a thin vapor layer [see Fig. 4(c), corresponding to the initial foil temperature of 300°C]. In this case cooling is practically impossible due to the absence of a direct contact between the liquid and the hot surface.

B. Drop impact onto hot steel foils coated by nanofiber mats: The inverse-Leidenfrost effect

In this subsection the outcomes of water and ethanol drop impacts onto a steel foil coated with a PAN+CB nanofiber mat with a thickness of $h = 0.5$ mm are illustrated and compared with the observations of the drop impact onto bare foils discussed in Sec. III A. Figure 5 shows the time sequences for water drop impacts onto the nanofiber-coated foil at different initial foil temperatures. While the first four images of every sequence were recorded with a frame rate of 30 000 fps, the last images were taken with the frame rate of 125 fps under identical experimental conditions. In order to allow comparison with the results of drop impact onto a bare foil, the same initial foil temperatures as in Fig. 3 were chosen. Figure 5(a) illustrates the outcome of water drop impact onto a nanofiber-coated foil with the initial temperature of 60°C. The image sequence demonstrates the typical drop impact behavior on nanofiber mats as described in Refs. [20,23]. Driven by the kinetic energy of impact, the drop spreads over the surface in the early stage of impact, as

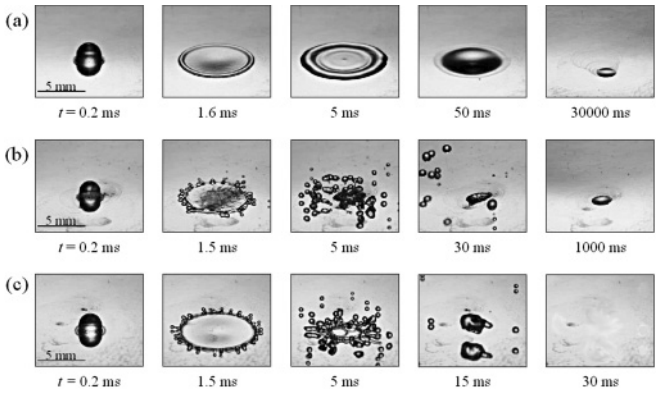

FIG. 4. Ethanol drop impact on a bare steel foil at different initial temperatures. The initial foil temperature $T_{\text{foil,init}}$ is equal to (a) 60°C, (b) 180°C, and (c) 300°C.

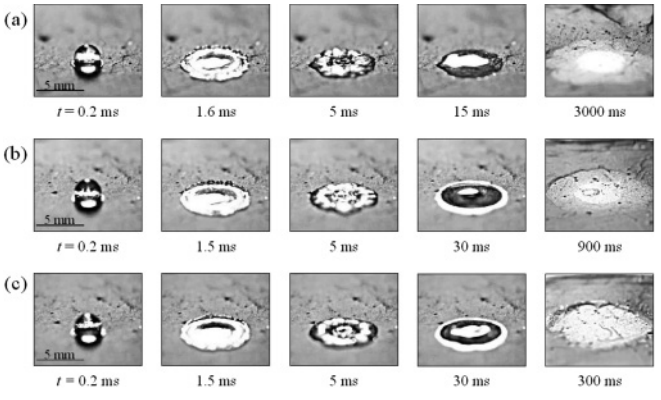

FIG. 5. Water drop impact onto PAN+CB nanofiber mat with thickness $h = 0.5$ mm at different initial temperatures of the underlying stainless steel foil. The initial foil temperature $T_{\text{foil,init}}$ is equal to (a) 60°C, (b) 220°C, and (c) 300°C.

it would do on an impermeable surface [23]. The observed morphological transformation of the drop at the earlier impact time coincides with the description of Ref. [26] for the case of the impermeable solid surfaces. On the other hand, the receding motion of the drop after impact does not arise on a nanofiber mat. The contact line is pinned at the maximum spreading position. After some time the drop starts to spread inside the nanofiber mat. The penetration of the liquid into the nanofiber mat and its spreading inside the mats has been investigated in Refs. [20,23]. The area of the nanofiber mat impregnated with water beyond the maximal spread-out spot can be seen in the last image of Fig. 5(a). This area is recognizable as a ring-shaped region which appears lighter than the dry mat.

This drop pinning observed on electrospun nano-textured surfaces has an intriguing physical reason [20,23]. Pore sizes in the mats are of the order of $d \approx 1\ \mu$m, whereas drop sizes are of the order of $D \approx 100 - 1000\ \mu$m. The motion of a massive drop impacting onto a nanofiber mat with a velocity V_0 (of the order of 1 m/s) is abruptly stopped by the surface. A part of its kinetic energy is redirected along the top surface as the drop spreads out and is gradually converted into surface energy or dissipated due to viscosity as the drop spreads. The other part of the drop kinetic energy is channeled into a few pores of the nano-textures surface. Because the drop and pore size are incommensurate, such channeling of the kinetic energy of a big drop into a few tiny pores results in the initial velocity U of pore filling much higher than V_0, namely $U \approx (D/d)V_0$ [20,23]. High values of U are kindred to the high speeds of Munroe' jets studied, in particular, in the seminal work of G. I. Taylor and coworkers [27], and widely used in ballistic penetration. They are much larger than the wettability-related Lucas-Washburn [28] velocity $V_{\mathrm{LW}} = \sigma d\cos\theta/(8\ \mu\mathrm{H})$, where σ and μ are the surface tension coefficient and viscosity of water, respectively, and θ is the contact angle. Therefore, water can penetrate into the nanofiber mat pores, irrespective of their wettability and fill the pores under the entire wetted spot visible above the surface. That also explains why a spread-out drop becomes pinned on nano-textured mats: It becomes a circular millipede.

Figures 5(b) and 5(c) show the outcomes of water drop impacts onto nanofiber-coated foils at initial temperatures of 220° and 300°C, respectively. It can be seen that the initial foil temperature has a negligible effect on the outcome of drop impact on nanofiber mats. In both cases water drops spread out as at the lower initial foil temperatures, do not shatter, and stay in full contact with the substrate. Breakdown of the spreading lamella, drop fragmentation, or levitation as in the case of drop impact onto bare steel foils do not occur on the surface coated with nanofiber mat. One of the noticeable changes in comparison with drop impact onto unheated nanofiber mats is in complete pinning of the drop contact line after reaching the maximum spreading configuration for higher temperatures. A puddle of liquid resting above the nanofiber mat decreases with time and eventually disappears, which happens partially due to its penetration and spreading inside the mat and partially due to evaporation. The time that elapses before the puddle disappears decreases with increasing foil temperature, as can be seen in the last image of every sequence in Fig. 5.

In Fig. 6 the observations of ethanol drop impacts onto nanofiber-coated foils are shown. Slight differences between

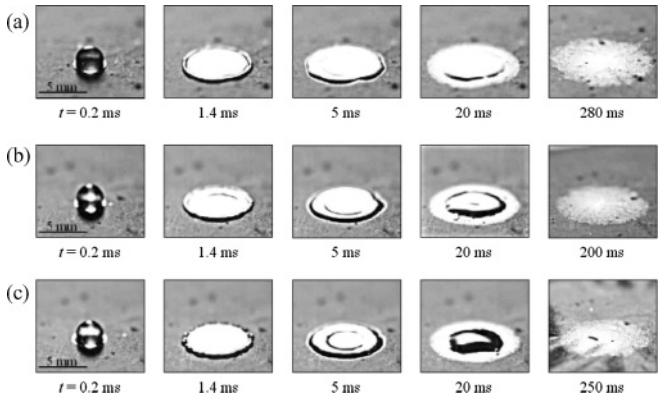

FIG. 6. Ethanol drop impact onto PAN+CB nanofiber mat with thickness $h = 0.5$ mm at different initial temperatures of the underlying foil. The initial foil temperature $T_{\mathrm{foil,init}}$ is equal to (a) 60°C, (b) 180°C, and (c) 300°C.

the behavior of the ethanol drops compared to that of the water drops can be seen in the case of the initial foil temperature $T_{\mathrm{foil,init}} = 60$°C. The ethanol drop spreads wider than the corresponding water drop since the surface tension of ethanol is lower than that of water. Comparison between the third and fourth image of every sequence reveals that the radius of the portion of the liquid that rests over the mats as a sessile drop decreases with time. It is also clearly seen that the time elapsing before the puddle resting over the mat disappears is much shorter for the ethanol drop in comparison with the water drop. It can be seen in Figs. 6(b) and 6(c) that the presence of the nanofiber mat completely eliminates the Leidenfrost effect of ethanol drops at the initial foil temperatures of 180° and 300°C [cf. with the corresponding Figs. 4(b) and 4(c)]. The overall behavior of ethanol drops after impacts on nanofiber-coated foils at the different initial foil temperatures is practically identical. Neither bubble formation in the nucleate boiling regime nor drop scattering and the Leidenfrost regime emerge. It can be concluded that the presence of nanofiber mats suppresses the Leidenfrost effect. Moreover, when the millipede-like Wenzel state is dynamically imposed by drop impact, nanofiber mats are capable of preserving it in spite of significant surface temperatures, whereas ordinary micropatterned substrates loose Wenzel state and transfer to the Cassie-Baxter state as in Ref. [29].

It is emphasized that the present experiments do not allow elucidation of the vapor outflow from nanofiber mats. Our preliminary numerical simulations show that vapor pressure field inside the mat under the location of drop impact in contact with a hot foil is prone to formation of the peripheral high pressure zones where vapor can escape partially or completely through the interfiber pores. The rate of vapor outflow is definitely strongly affected by the mat permeability, which can be estimated as $d^2/8$ where d is the pore size.

C. Effect of nanofiber mat on cooling efficiency

When a liquid drop comes in contact with a hot surface, the temperature of the surface in the contact area is reduced due to heat conduction between the hot foil and the cold drop and the latent heat of evaporation. At the nano-textured surfaces (coated with nanofibers) the anti-Leidenfrost effect results in

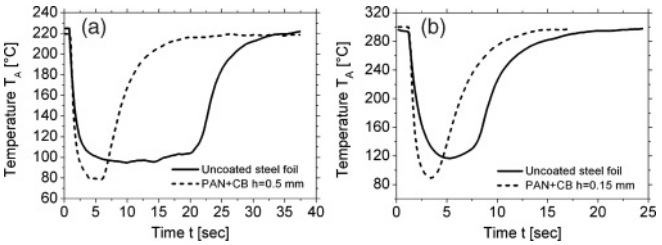

FIG. 7. Evolution of foil temperature under the drop impact point, T_A, for water drop impact. The initial foil temperature $T_{foil,init}$ is equal to (a) 220°C and (b) 300°C.

a wider wetted spot, suppresses liquid atomization, and thus increases the amount of liquid evaporating in direct contact (through the filled pores) with the underlying hot surface. Both the increase of the area from which the liquid evaporates and shorter evaporation time increase the heat removal rate and, thus, increase the cooling efficiency. This is illustrated by the results of the temperature measurements depicted in Figs. 7 and 8. In Fig. 7 the foil temperature evolution following water drop impact onto a bare steel foil is compared with the temperature evolution resulting from the drop impact onto a PAN+CB nanofiber mat of thickness $h = 0.5$ mm. The results are presented for the initial foil temperatures of 220° and 300°C.

Two main effects of the nanofiber mat can be observed in Fig. 7(a). The first effect is the reduction of the minimum temperature of the foil in the case of the nanofiber-coated foil in comparison with the uncoated foil. The minimal temperature is about 15°C lower in the case of the nanofiber compared with that of the bare steel foil. The second effect is the reduction of drop evaporation time on nanofiber mats. It is determined using the time during which the foil temperature is lower than the initial temperature. The evaporation time is about 15 s shorter on the nanofiber mats compared to that of the bare steel foil.

The temperature trends are qualitatively similar to the results reported in Refs. [21–23] for lower temperatures. The present work shows that the main features of drop impact onto nanofiber-coated surfaces do not change, at least up to initial foil temperatures of 300°C, as can be seen in Fig. 7(b). In the latter case the minimum temperature of the foil is about 20°C lower for the nanofiber-coated foil than that for the uncoated foil.

In Fig. 8 the foil temperature variation is plotted for the case of the ethanol drop impact onto a bare steel foil and onto a nanofiber-coated steel foil. The foil temperature trends on bare and nanofiber-coated foils for an initial temperature of 140°C for the ethanol drop impacts [Fig. 8(a)] are similar to the results for water drops. The minimal temperature of the nanofiber-coated foil is lower by about 15°C compared to the bare foil. The evaporation time on the nanofiber-coated surface is shorter compared to the bare steel surface. The Leidenfrost regime has not been reached yet at this initial foil temperature.

It has been shown in Fig. 4(b) that at the initial foil temperature of 180°C the ethanol drop impacting onto the bare foil shatters into smaller droplets which levitate above the foil surface. Only a small residual drop is left on the surface about 1 ms after first contact between the drop and the foil surface. Such drop shattering results in a drastic

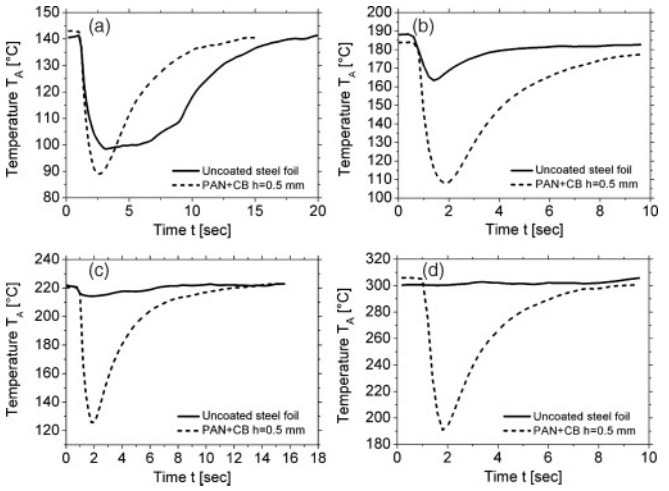

FIG. 8. Evolution of foil temperature under the drop impact point, T_A, for the ethanol drop impact. The initial foil temperature $T_{foil,init}$ is equal to (a) 140°C, (b) 180°C, (c) 220°C, and (d) 300°C.

deterioration of the cooling efficiency for drops impacting onto bare foil. Indeed, the minimal foil temperature achieved by the ethanol drop impact at 180°C is as high as 163°C [cf. Fig. 8(b)], whereas with the nanofiber mat coating the minimal temperature is about 110°C. This result is consistent with the behavior of the impacting ethanol drops as discussed in Sec. II [cf. Fig. 6(b)]. The ethanol drop impacts onto the bare foil surface at the initial temperatures of 220° and 300°C exhibit negligible cooling, which is the result of the Leidenfrost effect. Indeed, in these cases there is no direct contact between the hot surface and the drop. In contrast, the ethanol drop impacts onto the nanofiber-coated foil result in a reduction of the initial foil temperature by 95° and 115°C (for the initial temperatures of 220° and 300°C, respectively). This result illustrates that in the case of the ethanol drops the Leidenfrost effect is eliminated on the nanofiber-coated foil surface. Due to the presence of the nanofiber mats, direct contact between the liquid and the hot surface occurs and leads to a drastic reduction in the foil temperature.

The cooling effect of the drop impacts onto the nanofiber-coated and bare steel foils is summarized in Fig. 9, where the minimum foil temperature as a function of the initial foil temperature is plotted. The results for the water drop impact are shown in Fig. 9(a). It can be seen that the minimum temperature is reduced by using the nanofiber-coated foil for the range of initial foil temperatures 60–300°C. The improvement of the cooling efficiency is more significant at elevated temperatures.

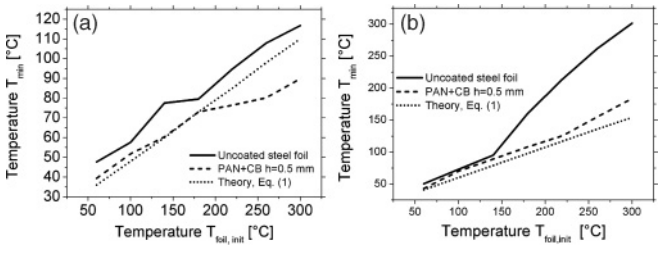

FIG. 9. Minimum foil temperature after drop impact as a function of the initial foil temperature for (a) water and (b) ethanol.

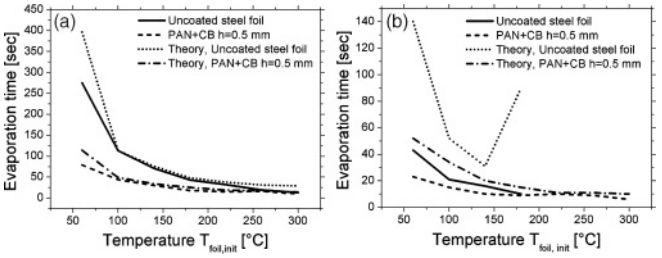

FIG. 10. Drop evaporation time on nanofiber-coated foils compared to the one on bare foils for (a) water and (b) ethanol.

The results for the ethanol drop impact depicted in Fig. 9(b) differ qualitatively. Although the improvement of the cooling efficiency at nanofiber-coated foils can be observed over the entire range of the tested initial foil temperatures, the drastic effect of the coating begins only at an initial foil temperatures above 180°C. This effect results in a temperature reduction of up to 115°C. The dramatic reduction of the foil temperature is achieved due to the anti-Leidenfrost effect associated with the nano-textured coating.

The thermal energy balance in the form of Eq. (17) in Ref. [23] suggests the following relation between $T_{\min}$ and $T_{\text{foil,init}}$

$$T_{\min} = \left(1 + \frac{\rho_{\text{steel}} c_{\text{steel}} h}{\rho_\ell c_\ell h_{\text{drop,resid}}}\right)^{-1} \times \left(\frac{\rho_{\text{steel}} c_{\text{steel}} h}{\rho_\ell c_\ell h_{\text{drop,resid}}} T_{\text{foil,init}} + T_{\text{drop,init}}\right), \quad (1)$$

where $h_{\text{drop,resid}}$ is the residual thickness of the spread-out drop, ρ and c are the density and specific heat, respectively, and subscripts ℓ and steel refer to liquid and foil, respectively; $T_{\text{drop,init}}$ is the initial drop temperature.

The comparison of Eq. (1) with the experimental data in Fig. 9 shows that the predictions are in a reasonably good agreement with the data for both liquids for nanofiber mats approximately up to $T_{\text{foil,init}} = 200$°C. Above that temperature, flash evaporation or boiling can set in as the liquid film spreads over the nanofiber mat. These factors are not accounted for in Eq. (1) and can be responsible for the increasing deviation of the predictions from the data for nanofiber mats. On the other hand, the assumption of a spread-out liquid drop in good contact with the substrate embedded in Eq. (1) is absolutely inappropriate for drop impacts on bare foil at elevated temperatures. Therefore, Eq. (1) should not be able to describe the data for uncoated steel foil, and, indeed, Fig. 9 shows that this is the case.

The results on the drop evaparation time that was estimated from the foil temperature measurements are summarized in Fig. 10. It is seen that the drop evaporation time is reduced in the case of drop impact onto nanofiber-coated foils compared with the drop impact onto uncoated foils. This reduction corresponds to the spreading and pinning of liquids in the presence of nanofiber mats. The increase of the cooled area cannot be detected by the temperature measurements with a single thermocouple positioned under the drop impact point. However, the increase in the cooled area can be measured using the infrared thermography [23]. The difference in the evaporation time between the bare and nanofiber-coated foils

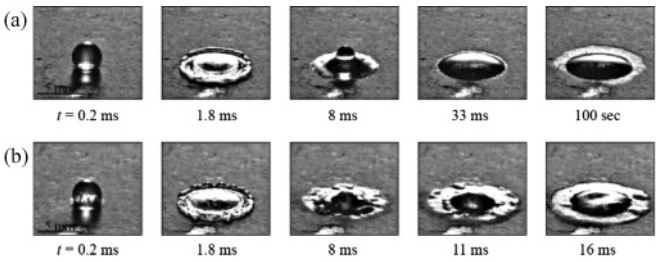

FIG. 11. Water drop impact on a PAN+CB nanofiber mat with thickness $h = 0.15$ mm. The initial foil temperature is equal to (a) 80°C and (b) 180°C.

decreases as the initial temperature increases. This can be caused by the enhanced bubble nucleation on bare foils at elevated temperatures. The latter, however, also enhances drop atomization, which reduces the evaporated liquid mass and thus heat removal from bare foils even though the residual drops evaporate as fast as on the nanofiber-coated foils. It has been impossible to measure the evaporation time of the drops in the Leidenfrost regime, since the drop impact results in negligible foil cooling and the evaporation time cannot be determined from the temperature measurements.

The evaporation time Δt was predicted using Eq. (19) from our previous work [23]. The comparison of the predictions with the experimental data is shown in Fig. 10. It is seen that for water the predictions agree with the data over the entire high temperature range: better for the nanofiber mat and worse for bare foil. On the other hand, for ethanol the theory deviates dramatically from the data (as expected) since the Leidenfrost effect sets in on the bare foil. On the contrary, the predictions and the data for ethanol on the nanofiber mat in the inverse-Leidenfrost regime exhibit good agreement.

IV. ADDITIONAL OBSERVATIONS

A. Too-thin mats or too-big drops

In some cases nanofiber mats were too thin to rapidly accommodate most of the liquid protruding into pores after a drop impact. As a result, most of the liquid delivered by a drop stayed above the mat surface for some time in a spread-out configuration after the initial impact-triggered spreading i.e. puddles were formed. Different wave patterns were observed on the puddle surfaces. Two examples are shown in Fig. 11, which shows the outcome of water drop impact onto a foil covered by a PAN+CB mat of 0.15-mm thickness. In the case of an initial foil temperature of 80°C the drop spread after the impact until its maximum spreading diameter was reached and the contact line pinned. After that the liquid in the puddle was oscillating above the area encircled by the contact line until the kinetic energy of the standing wave was consumed. The

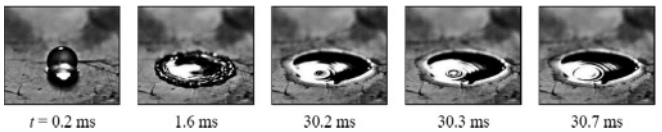

FIG. 12. Water drop impact onto a damaged PAN nanofiber mat with thickness $h = 1.5$ mm. The initial foil temperature is equal to 220°.

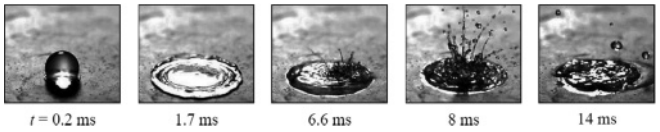

FIG. 13. Water drop impact onto a damaged PAN nanofiber mat with a thickness $h = 0.25$ mm. The initial foil temperature is equal to 220°C. This sequence of images illustrates the formation of a geyser.

free surface was rather smooth [Fig. 11(a)]. The liquid from the puddle was penetrating into the pores at a rate limited by the evaporation inside the mat, which took a longer time than the standing wave oscillations [cf. Fig. 11(a)].

On the other hand, at a higher initial foil temperature of 180°C the puddle surface roughens in the course of the standing wave oscillations at about 8 ms after the impact [cf. Fig. 11(b)], which suggests bubble formation inside the nanofiber mat due to the intense evaporation at this elevated temperature. The rate of liquid penetration from the puddle into the pores is still limited by the evaporation rate, which is much higher in this case than in Fig. 11(a). Then, the corresponding penetration process is much shorter [compare Figs. 11(a) and 11(b)].

B. Damaged mats: Inhomogeneous bubbling and geysers

The mat shown in Fig. 12 was first used in the experiments with the anti-Leidenfrost effect at 250°C described in Sec. III. Presumably, due to significant and long evaporation inside this nanofiber mat in those experiments, some damage in its internal architecture resulted. When this nanofiber mat was used again, the formation of circular waves emanating from a certain location at the mat surface was observed (see Fig. 12). The waves were seemingly induced by a hole in the nanofiber mat at $t = 30.2$ ms that suddenly appeared. The pattern observed was seemingly triggered by a vapor bubble released through the damaged location in the mat.

Another mat was initially used in the experiments with the anti-Leidenfrost effect at 250°C described in Sec. III, and demonstrated a regular behavior. When it was reused later at a temperature of 220°C, the unusual pattern shown in Fig. 13 was observed. While the drop spreading looked normal at 1.7 ms, the accelerated water jets started to break through the free surface at 6.6 ms after drop impact (Fig. 13). They continued for a while but then they finally collapsed and broke up into small droplets. Presumably, the internal mat architecture was damaged during extended boiling in the first series of the experiments, which caused a localized instantaneous failure inside the mat during the time interval 1.7 ms $< t <$ 6.6 ms. This triggered the formation of the geyser seen in Fig. 13.

V. CONCLUSION

A suppression of the Leidenfrost effect is presented in this arcticle. Polymer nonwoven nanofiber mats were created and deposited by electrospinning onto heatable stainless steel foils. It has been demonstrated that the presence of a nanofiber mat dramatically changes drop impact hydrodynamics. No receding motion, bouncing, or Leidenfrost levitation and skittering over the hot surface occur after the drop impact onto nanofiber-coated hot foils. The temperature measurements indicated a significant cooling effect of drop impact onto nanofiber-coated surfaces at elevated temperatures. The temperature measurements confirmed the fact that after impact liquid penetrates into the mats and stays as a circular milliped in direct contact with the hot surface. The anti-Leidenfrost effect has been most pronounced for ethanol drop impact, in which case using the nanofiber coating leads to a reduction of a foil temperature from 300° to 190°C, whereas the impact of an ethanol drop onto a bare steel foil heated up to 300°C produced no cooling effect. The results show that using nanofiber-coated foils holds promise for drop or spray cooling of high power electronic devices at elevated temperatures and can lead to a breakthrough in the cooling technologies. This is also corroborated by tremendously high heat removal rates of about 0.6 kW/cm^2 achieved on metal-plated nanofiber mats in the accompanying paper [22]. The physical mechanism of the inverse-Leidenfrost effect on nanofiber-coated mats is determined by pinning the drop contact line in the spread-out configuration and maximal suppression of liquid atomization from the wet spot even at very high temperature.

ACKNOWLEDGMENTS

Partial support of Y.Z., S.S.-R., and A.L.Y. by the NSF (Grant No. CBET 0966764) and NASA (Grant No. NNX10AR99G) is greatly appreciated. This work was partially funded by the Deutsche Forschungsgemeinschaft through the Center of Smart Interfaces.

[1] J. G. Leidenfrost, *De Aquae Communis Nonnullis Qualitatibus Tractatus* (University of Duisburg, Duisburg, 1756).
[2] J. Tindall, *Heat as a Mode of Motion* (D. Appleton and Company, New York, 1863).
[3] J. Child, COTS J. **2**, 1 (2009).
[4] D. Kinney, COTS J. **2**, 3 (2009).
[5] A. L. Yarin, Annu. Rev. Fluid Mech. **38**, 159 (2006).
[6] V. G. Labeish and A. G. Pimenov, J. Eng. Phys. Thermophys. **47**, 1400 (1984).
[7] Y. S. Ko and S. H. Chung, Exp. Fluids **21**, 118 (1996).
[8] A. Karl and A. Frohn, Phys. Fluids **12**, 785 (2000).
[9] G. E. Cossali, M. Marengo, and M. Santini, Exp. Thermal Fluid Sci. **29**, 937 (2005).
[10] I. V. Roisman, J. Fluid Mech. **656**, 189 (2009).
[11] B. S. Gottfried, C. J. Lee, and K. J. Bell, Int. J. Heat Mass Transf. **9**, 1167 (1966).
[12] A. L. N. Moreira, A. S. Moita, and M. R. Panão, Prog. Energy Combust. Sci. **36**, 554 (2010).
[13] A. -L. Biance, C. Clanet, and D. Quéré, Phys. Fluids **15**, 1632 (2003).

[14] A. Biance, F. Chevy, C. Clanet, G. Lagubeau, and D. Quéré, J. Fluid Mech. **554**, 47 (2006).
[15] L. Xu, Phys. Rev. E **75**, 056316 (2007).
[16] M. Ojha, A. Chatterjee, F. Mont, E. F. Schubert, P. C. Wayner Jr., and J. L. Plawsky, Int. J. Heat Mass Transf. **53**, 910 (2010).
[17] C. Sodtke and P. Stephan, Int. J. Heat Mass Transf. **50**, 4089 (2007).
[18] D. H. Reneker, A. L. Yarin, E. Zussman, and H. Xu, Adv. Appl. Mech. **41**, 43 (2007).
[19] D. H. Reneker and A. L. Yarin, Polymer **49**, 2387 (2008).
[20] A. N. Lembach, H. B. Tan, I. V. Roisman, T. Gambaryan-Roisman, Y. Zhang, C. Tropea, and A. L. Yarin, Langmuir **26**, 9516 (2010).
[21] R. Srikar, T. Gambaryan-Roisman, C. Steffes, P. Stephan, C. Tropea, and A. L. Yarin, Int. J. Heat Mass Transf. **52**, 5814 (2009).
[22] S. Sinha-Ray, Y. Zhang, and A. L. Yarin, Langmuir **27**, 215 (2011).
[23] C. M. Weickgenannt, Y. Zhang, A. N. Lembach, I. V. Roisman, T. Gambaryan-Roisman, A. L. Yarin, and C. Tropea, Phys. Rev. E **83**, 036305 (2011).
[24] D. H. Reneker, A. L. Yarin, H. Fong, and S. Koombhongse, J. Appl. Phys. **87**, 4531 (2000).
[25] J. Senda, K. Yamada, H. Fujimoto, and H. Miki, JSME Int. J. **31**, 105 (1988).
[26] R. Rioboo, M. Marengo, and C. Tropea, Exp. Fluids **33**, 112 (2002).
[27] G. Birkhoff, D. P. Macdougall, E. M. Pugh, and G. I. Taylor, J. Appl. Phys. **19**, 563 (1948).
[28] E. W. Washburn, Phys. Rev. **17**, 273 (1921).
[29] G. Liu, L. Fu, A. V. Rode, and V. S. J. Craig, Langmuir **27**, 2595 (2011).